Article

Microstructure Evolution during High-Pressure Torsion in a 7xxx Series Al-Zn-Mg-Zr Alloy

Anwar Qasim Ahmed , Dániel Olasz , Elena V. Bobruk , Ruslan Z. Valiev , Nguyen Q. Chinh *

Posted Date: 29 December 2023

doi: 10.20944/preprints202312.2105.v1

Keywords: AlZnMg alloy; HPT; UFG; TEM; DSC; hardness; tensile test; decomposition; GB segregation; superplasticity

Article

Microstructure Evolution during High-Pressure Torsion in a 7xxx Series Al-Zn-Mg-Zr Alloy

Anwar Qasim Ahmed [1,2], Dániel Olasz [1,3], Elena V. Bobruk [4], Ruslan Z. Valiev [4,5] and Nguyen Q. Chinh [1,*]

[1] Department of Materials Physics, ELTE Eötvös Loránd University, Pázmány Péter sétány 1/A, Budapest, 1117 Hungary; anwar.ahmed.qasim@gmail.com (A.Q.A.); olasz.dani96@gmail.com (D.O.); chinh@metal.elte.hu (N.Q.C.)
[2] College of Science, University of Kufa, Najaf, 54001 Iraq
[3] Institute for Technical Physics and Materials Science, Centre for Energy Research, Budapest Konkoly-Thege út 29-33, Budapest, 1121 Hungary
[4] Institute of Physics of Advanced Materials, Ufa University of Science and Technology, 32 Zaki Validi str., Ufa, 450076 Russia; e-bobruk@yandex.ru (E.V.B.); ruslan.valiev@ugatu.su (R.Z.V.)
[5] Laboratory for Dynamics and Extreme Performance of Advanced Nanostructured Materials, Saint Petersburg State University, St. Petersburg, 199034 Russia
* Correspondence: chinh@metal.elte.hu

Abstract: A homogenized, supersaturated Al-Zn-Mg-Zr alloy was processed by severe plastic deformation (SPD) using high-pressure torsion (HPT) technique for different revolutions at room temperature to get ultrafine-grained (UFG) microstructure. The microstructure and mechanical properties of the UFG samples were then studied by transmission electron microscopy (TEM), differential scanning calorimetry (DSC), as well as by tensile and hardness measurements. Emphasis was placed on the effect of shear strain on the evolution of microstructure of the investigated alloy. Experimental results have shown a very interesting evolution of the decomposed microstructure in a wide range of shear strains imposed by HPT. While the global properties, such as the average grain size (~200 nm) and hardness (~2.2 GPa) appeared unchanged, the local microstructure was continuously transformed. After 1 turn of HPT, the decomposed UFG structure contains relatively large precipitates inside grains. In the sample processed by 5 turns in HPT, segregation of Zn atoms into grain boundaries (GBs) can also be observed. After 10 turns, more Zn atoms have segregated into GBs and only smaller size precipitates can be observed inside grains. The intensive segregation of solute atoms into GBs may significantly affect the ductility of the materials, leading to its ultralow-temperature superplasticity. Our findings pave the way for achieving advanced microstructural and mechanical properties in nanostructured metals and alloys by engineering their precipitation and segregation by means of applying different HPT regimes.

Keywords: AlZnMg alloy; HPT; UFG; TEM; DSC; hardness; tensile test; decomposition; GB segregation; superplasticity

1. Introduction

In recent decades, many researchers in the material physics field have devoted their efforts to study the effect of Severe Plastic Deformation (SPD) on the mechanical and microstructure properties of the different alloys. Among the numerous SPD processes, High-Pressure Torsion (HPT) [1,2] is a considerable and widely applied method for investigating the significance of SPD on metallic alloys. Enormous shear strain of this technique produces an ultrafine-grained (UFG) structure and may result in the formation of nanoprecipitates in the processed materials [3-7]. In this regard, the mechanical and microstructure characteristics of UFG materials processed by HPT are affected also by the dissolving and precipitating of nanosized-dispersoid, in addition to the effect of the density of defects [8-10]. It is also well known that a significant amount of shear strain in HPT may cause the dynamic recovery and recrystallization of precipitates [11-15]. The effect of this phenomenon has previously been studied in many works [16-19]. Previous studies for the dynamic precipitation

 doi:10.20944/preprints202312.2105.v1

behavior in the HPT-processed alloy demonstrate that decomposed solid solution at RT creates nanoscale solute structures in the matrix associated with the segregation of solute atoms at the GBs. These structures work in conjunction with the grain refinement effect and high dislocation density to improve the strength of HPT-processed alloy by suppressing grain growth during dynamic recrystallization [20]. Moreover, HPT has a significant potential to produce non-equilibrium GBs microstructures that have a relatively high grain boundary energy, thereby improving the segregation at GBs during the SPD process [6,7,15]. These findings demonstrate that the SPD technique is a magnificent method for designing a UFG microstructure of an Al alloy by driving grain refinement, dynamic reversion, and solute heterogeneity precipitations.

It is well known that the AlZnMg chemical composition (7xxx) alloys have been considered as the most significant basic materials in the Al industry. These materials are widely investigated due to their excellent mechanical properties [7-21], as the initially supersaturated microstructure can be varied conveniently by applying different heat treatments and plastic deformation techniques.

Despite extensive investigations, the effect of the different shear strains imposed in HPT processes on same the microstructure and on the subsequent mechanical properties of several Al-Zn-Mg alloys has not been clarified in detail.

The aim of this work is to investigate the microstructure evolution of an Al-4.8%Zn-1.2%Mg-0.14%Zr (wt.%) processed by HPT and its effect on mechanical properties by using depth-sensing indentation (DSI), transmission electron microscope (TEM) and differential scanning calorimeter (DSC), as well as by microhardness and tensile measurements.

2. Materials and Methods

The alloy with a weight percent composition of Al-4.8Zn-1.2Mg-0.14Zr was firstly processed by casting. Then, the material was homogenized at 470 °C for 8 h, and hot extruded at 380 °C. In the following step, disks having diameter of 20 mm and a thickness of 1.4 mm were cut from the extruded rods and processed by high-pressure torsion (HPT). Prior to HPT processing, the disk-samples were again homogenized at 470 °C for 1 h and then water-quenched to room temperature (RT). The disks were subjected to N = 1, 2, 5 or10 revolutions (turns) of HPT at RT under a pressure of 6 GPa. Samples taken at the half-radius of the HPT disks were used for further investigations, where the samples will be identified as HPT-1, HPT-2, HPT-5 and HPT-10, according to the number of revolutions in the HPT process. Details of the HPT process can be found elsewhere [1,2].

The microstructure of the samples was investigated using transmission electron microscopy (TEM). A Titan Themis G2 200 scanning transmission electron microscope (STEM) was used for TEM and energy-disperse X-ray spectroscopy (EDS) investigations. The STEM images were taken by a high-angle annular dark-field (HAADF) detector. Some experimental results on the microstructure of the sample HPT-10 have already been published before [22]. In order to identify the thermal events, differential scanning calorimetry (DSC) of Perkin-Elmer type equipment was used at heating rates of 10, 20, 30 and 40 K/min.

Mechanical properties of the samples were followed by performing tensile and microhardness tests. The tensile measurements were conducted at testing temperature of 170 °C and strain rate, $\dot{\varepsilon}$ of $5 \times 10^{-4}\,s^{-1}$ by using an Instron 5982 machine. Microhardness tests were carried out by depth-sensing indentation using a Vickers indenter tip for maximum loads of 50 mN and applying the well-known Oliver-Pharr method [23,24].

3. Results

3.1. Effect of HPT on Mechanical Properties of AlZnMgZr Samples

Figure 1 shows the Vickers microshardness values, HV of the investigated AlZnMgZr samples after different turns (N) of HPT processing. For the purpose of comparison, the hardness of the initial (Q) sample, as well as the hardness of the un-deformed sample, which was stored at room temperature (naturally aged) for a long time (more than 1 year). In this figure, the amount of shear strain (gamma) at a certain number of HPT evolutions is also plotted.

Preprints (www.preprints.org) | NOT PEER-REVIEWED | Posted: 29 December 2023 doi:10.20944/preprints202312.2105.v1

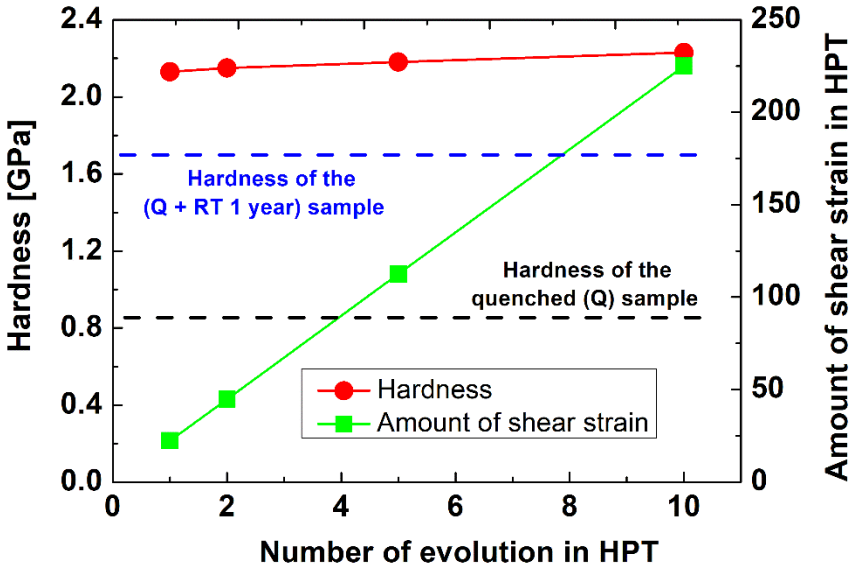

Figure 1. Microhardness of the investigated HPT-processed AlZnMgZr samples.

The experimental results indicate well the strengthening effect of HPT processing. Already after the first turn, the hardness of the sample reaches 2200 MPa, which is two and a half times higher than that (~830 MPa) of the freshly annealed sample, and approximately 30% higher than the hardness (~1700 MPa) of a sample naturally aged for a long time. Furthermore, it can be seen that the hardness of the HPT-processed samples is practically the same, regardless of the number of evolutions.

Figure 2 presents the creep behaviors of the different HPT-processed samples which were deformed by tensile tests performed at strain rate of $5 \times 10^{-4} s^{-1}$ and testing temperature of 170 °C. Even though their hardness at room temperature is almost the same, their creep properties are significantly different and depend on the number of revolutions. It can be seen that while the maximum flow stress of the samples is decreasing (from 180 to 58 MPa), their maximum elongation is increasing (from 40 to 500%) with the increasing number of the evolutions in HPT, showing the superplasticity of the sample processed by HPT in 10 turns. It should be noted that the testing temperature of 170 °C is only $0.47T_m$, lower than half of the absolute melting point (T_m) of aluminum. The low-temperature superplasticity of the ultrafine-grained HPT-10 sample with a record elongation of 500% has been investigated in more detail before [7].

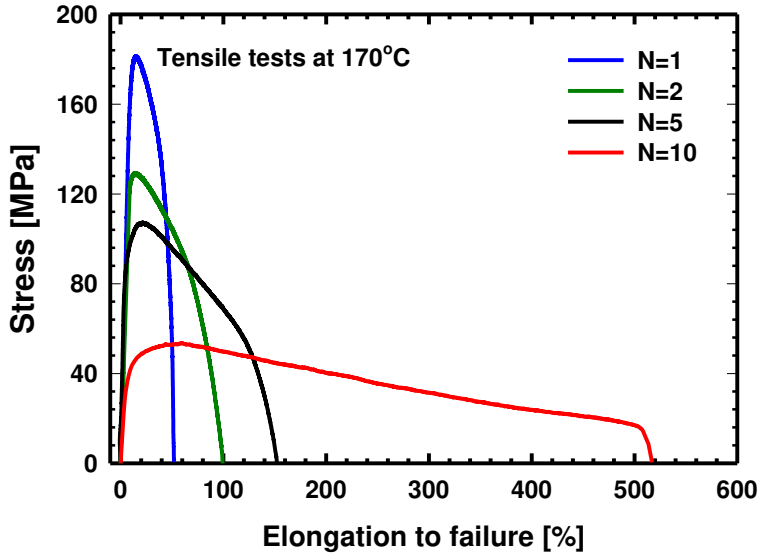

 doi:10.20944/preprints202312.2105.v1

Figure 2. Stress-elongation curves of the different HPT-processed samples deformed by tensile tests.

3.2. Effect of HPT on microstructure observed by TEM

The HPT processing has significantly modified the microstructure of the initially coarse-grained, supersaturated sample, where only Al_3Zr particles having size of 10-20 nm and finely distributed Guinier-Preston (GP) zones can be found [6]. Figure 3. shows the TEM images in HAADF mode on the HPT-1 (Figure 3a) and HPT-5 (Figure 3b) samples. Figure 4 shows the microstructure of the HPT-10 sample with more details.

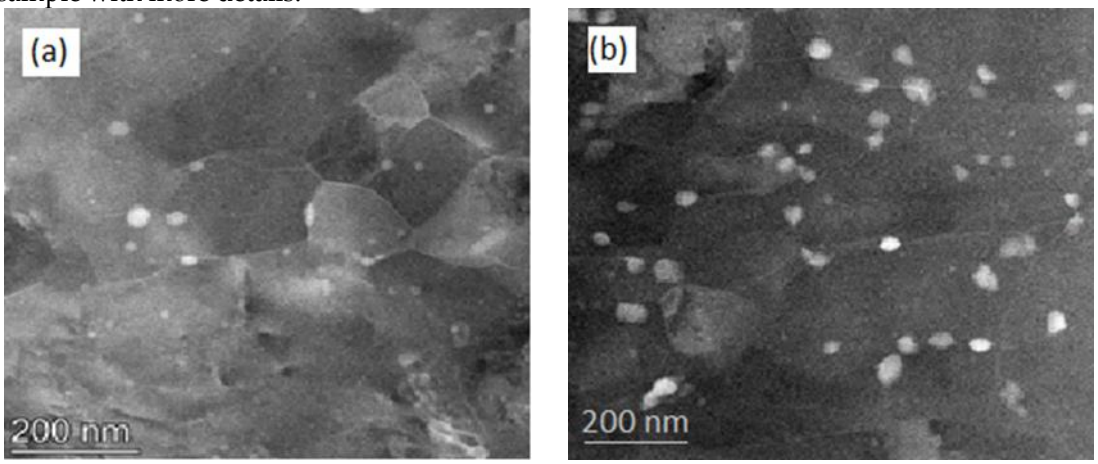

(**a**) (**b**)

Figure 3. STEM-HAADF images on the microstructures of **(a)** HPT-1 and (**b**) HPT-5 samples.

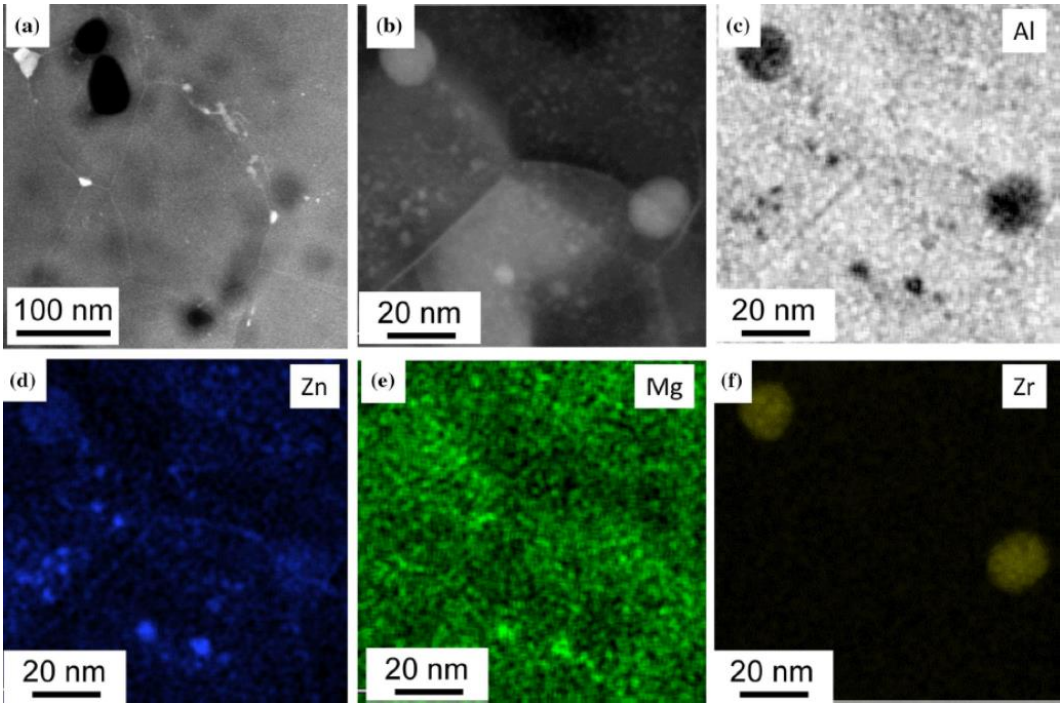

Figure 4. UFG microstructure of the investigated HPT-10 sample taken as (**a–b**) HAADF STEM images in low and higher magnifications, respectively, and (**c–f**) corresponding EDS elemental maps obtained on the area shown in (**b**), indicating the present of small Mg/Zn precipitates together with two Al_3Zr particles. Reproduced from Ref. [22]. Copyright 2020, Springer.

Experimental results show very clearly the grain-refining effect of the HPT process, which resulted in ultrafine-grained (UFG) structures having average grain size of about 200 nm in all investigated HPT-processed samples, leading to increment in the hardness of these HPT-processed

Preprints (www.preprints.org) | NOT PEER-REVIEWED | Posted: 29 December 2023 doi:10.20944/preprints202312.2105.v1

samples, as shown in Figure 1. Further careful investigations have shown that η-phase $MgZn_2$ precipitates can also be observed in the HPT-processed samples. These precipitates appear as bright areas on the HAADF-STEM images since the atomic number of Zn is much higher than that of Al. It can also be observed that the formation of the η-phase MgZn2 particles is significantly affected by the number of evolutions (the amount of shear strain) applied in HPT process. After one evolution (N =1) η-phase particles having size between 5 and 30 nm (see Figure 3a) are formed. After 5 evolutions more and somewhat larger particles can be observed in the size range of 20-40 nm (Figure 3b). It is interesting that after more severe shear strain in 10 evolutions in HPT, particles larger than 10-15 nm are rarely visible (see Figure 4a), rather much finer, only 2-5 nm particles can be observed (see the magnified TEM image of Figure 4b).

Given that the η-phase MgZn2 precipitates were mainly formed along or near the grain boundaries, this result suggests that during further deformation the particles are fragmented and/or partially dissolved into the matrix, changing the structure of the grain boundaries.

Figure 5 shows the HAADF image on a typical grain boundary (Figure 5a), together with corresponding energy-dispersive X-ray spectroscopy (EDS) maps (Figure 5b-d) and EDS line profile analysis (Figure 5e, f) observed in the HPT-10 sample. Experimental results reveal both the depletion of Al (Figure 5b), and the excess of Mg and Zn solue atoms (Figure 5c-f) in the grain boundaries of this sample. The results of EDS measurements have shown that most of grain boundaries in the HPT-10 sample can be regarded as Zn/Mg-rich boundaries. In the case of the HPT-5 sample, only a small fraction of the grain boundaries is segregated by Zn and Mg. The HPT-1 sample is not at all characterized by the presence of grain boundaries segregated by Zn and Mg solute atoms.

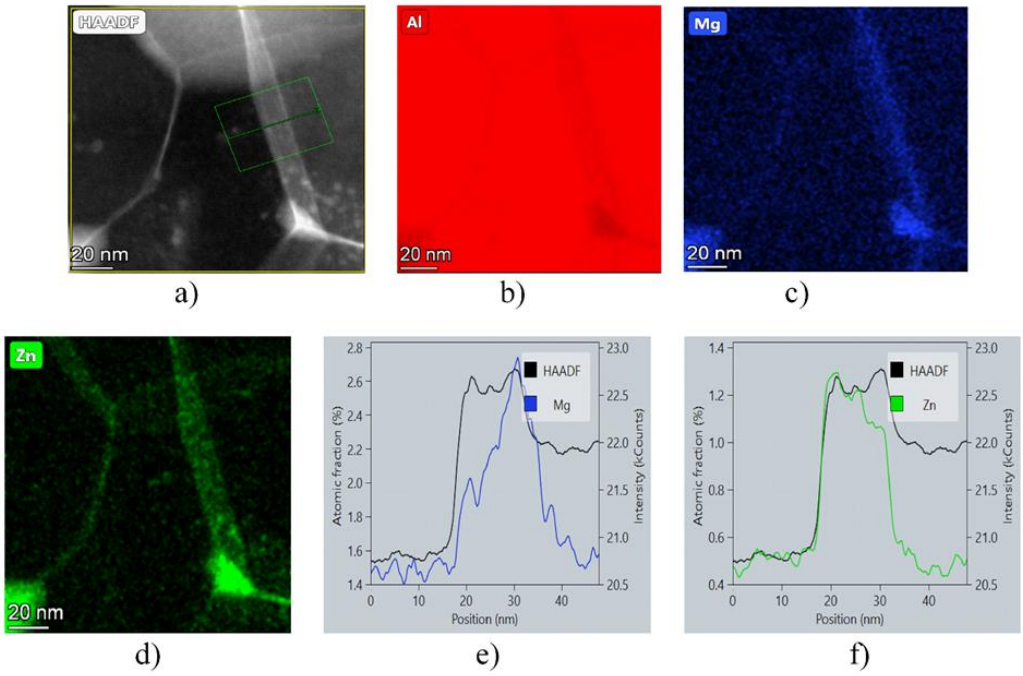

Figure 5. Typical grain boundary of HPT-10 sample shown by (**a**) HAADF image indicating Zn-rich (brightly imaged) boundaries, (**b–d**) corresponding element maps for Al, Mg and Zn, respectively. (**e**) and (**f**) EDS profile analysis along a boundary, revealing the segregation of Zn and Mg solute atoms into grain boundaries.

3.3. Characterization of Different HPT-Processed Microstructures by DSC Measurements

Figure 6 shows the DSC thermograms (heat flow-temperature curves) obtained at different heating rates (V) on the different (HPT-1, HPT-2, HPT-5 and HPT-10) samples in the testing temperature range from 300 to 760 K. In all cases, the thermograms can be characterized by the presence of three peaks. First, an endothermic peak is observed during the heating process, indicating the dissolution of existing phases in the UFG microstructure. Then, an exothermic peak is followed,

Preprints (www.preprints.org) | NOT PEER-REVIEWED | Posted: 29 December 2023 doi:10.20944/preprints202312.2105.v1

which is related to the precipitation and coarsening of precipitates. The third peak is another endothermic one observed at a higher temperature range, denoting the final dissolution process of precipitates formed through the whole heat treatment [25-27]. In the present work, where the focus is on the evolution of the microstructure during HPT processing, the characteristics of the first two (endo- and exothermic) we are primarily investigated and analyzed.

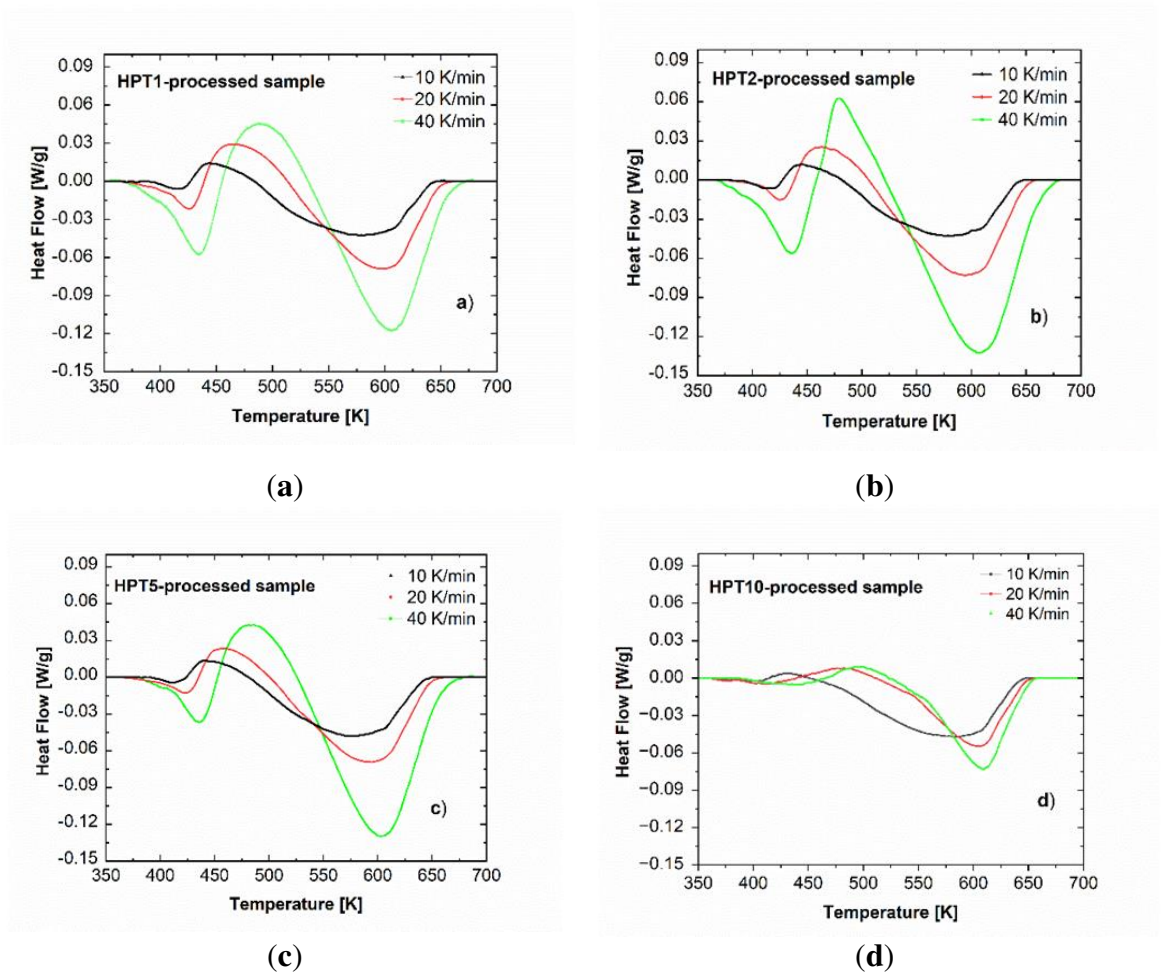

Figure 6. Typical DSC thermograms taken on (**a**) HPT-1, (**b**) HPT-2, (**c**) HPT-5 and (**d**) HPT-10 samples at different heating rates.

Using the experimentally measured DSC thermograms, both the specific heats (enthalpies) of the dissolution (for endothermic reaction), ΔH_d and that of precipitation (for exothermic reaction), ΔH_p can be determined. Experimental results have shown that at a given sample, these quantities obtained at different heating rates are almost the same. The quantities obtained in different samples indicate how the fraction of dissolved or formed phases change in these samples [6,28-29]. In the present work, the measured specific heats are listed in Table 1, showing well the tendency of the microstructure-evolution during HPT process.

Table 1. Specific enthalpy values, ΔH_d and ΔH_p obtained for the different HPT-processed Al-Zn-Mg-Zr samples. (The values are within 15% relative error).

Reaction type	HPT-1 sample	HPT-2 sample	HPT-5 sample	HPT-10 sample
Dissolution (endothermic), ΔH_d [J/g]	2.06	1.83	1.16	0.504
Precipitation	3.64	3.04		

Preprints (www.preprints.org) | NOT PEER-REVIEWED | Posted: 29 December 2023 doi:10.20944/preprints202312.2105.v1

(exothermic), ΔH_p [J/g]	3.02	0.65

3.3.1. The activation energy of transformation processes

It is well known that the transformation dynamic requires activation energy to diffuse their constituents of solutes in the microstructure through the reversion and precipitates processes. This energy value is changed greatly by modifying the microstructure via the SPD process. Because of thermal activation, the peak temperature, T_p of both the endothermic and exothermic peaks is shifted towards higher temperature when increasing the heating rate during DSC measurements. The activation energies for these reactions can be determined by applying the Kissinger equation [30-31]:

$$\ln\left(\frac{V}{T_p^2}\right) = C + \frac{Q}{RT_p}, \quad (1)$$

where V and T_p represent the heating rate (in K/min) and peak temperature, respectively of a given process, C is a material constant and R is the universal gas constant. The activation energy, Q will be denoted as Q_d for the dissolution, and as Q_p for the precipitation reactions.

Figure 7 shows the Kissinger plots obtained for the first dissolution (Figure 7a) and precipitation (Figure 7b) reactions in the investigated HPT-processed samples. In all cases, the data points can be fitted well with a linear line. According to Eq. (1) the activation energies for different processes can be determined from the slopes of the fitted lines, within 10% relative errors. The obtained values can also be seen in the figures.

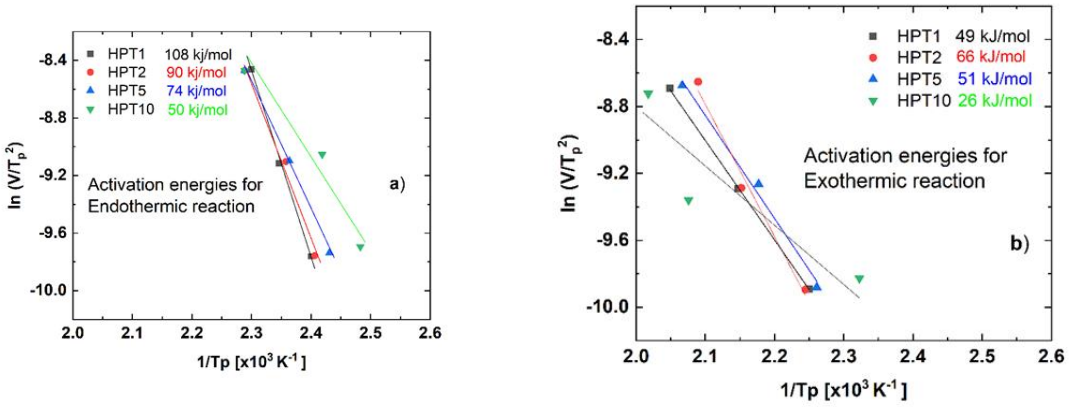

(**a**) (**b**)

Figure 7. Kissinger plots for (**a**) the first dissolution and (**b**) precipitation reactions in HPT-processed AlZnMgZr samples.

Experimental results show that both activation energies are affected significantly by the number of HPT revolutions. Increasing the number of the revolutions from 1 to 10, the activation energy characterizing the dissolution reaction (see Figure 7a) is monotonously decreasing from 108 to only 50 kJ/mol. At the same time, the activation energy value of precipitation process (Figure 7b) slightly decreases from 49 to 26 kJ/mol.

3.3.2. Kinetic parameters for different reactions during DSC measurements

It is well established that the kinetics of the dissolution and precipitation reactions taking place in the materials when imposed to DSC of non-isothermal heat treatment can be described by the kinetics parameters developed by the Avrami-Johnson-Mehl theory [31-32]. These quantities are represented by the transformed volume fraction, Y given by:

Preprints (www.preprints.org) | NOT PEER-REVIEWED | Posted: 29 December 2023 doi:10.20944/preprints202312.2105.v1

$$Y(T) = \frac{A(T)}{A(T_f)}, \tag{2}$$

and the rate of transformation, dY/dt which can be given as:

$$\frac{dY}{dt} = \frac{dY}{dT} \cdot \frac{dT}{dt} = \frac{dY}{dT} \cdot V, \tag{3}$$

at heating rate V. Here, $A(T)$ is the area under the given – endo or exothermic – peak in the range of temperature extended from the initial temperature, T_i to actual temperature, T. The T_f is the final temperature of the investigated peak in the DSC profile.

Figure 8 shows the experimentally determined Y-T plots characterizing the dissolution (Figure 8a-c) and precipitation (Figure 8d-f) in HPT-1, HPT-5 and HPT-10 samples measured at different heating rates. It can be seen that these sigmodal shape functions are shifted to a higher temperature as the shear strain increased by increasing the HPT revolution number and at increasing heating rate as well. The interval of temperature range which covers the endothermic reaction for the HPT-11 and HPT-5 samples appears slightly different. It is extended from around 390 to 457 K, i.e., extending over 67K. Further, for the HPT10-processed sample, this interval begins earlier, at 380K and finishes later, at 471K, extending over 91K, which it is one and a half times larger than that for the HPT-1 and HPT-5 samples. This behavior indicates that the dissolved precipitates in the HPT-10 samples) are less stable, so they dissolved earlier into the matrix. Furthermore, the beginning of the exothermic reaction in the HPT-10 sample is also slightly shifted towards lower temperature. It can be observed that the precipitation reaction started at 434K and 420K for the HPT-1 and HPT-10 samples, respectively, indicating the easier precipitation in the HPT-10 sample.

Figure 9 shows the change of the transformation rate, dY/dt in the function of temperature for the HPT-1, HPT-5 and HPT-10 samples. It can be seen that the transformation rate is low at the beginning and at the end of the given process, and there is a rapid increment in between, showing a maximum located in the middle region. In the case of endothermic reactions (Figure 9a-c), the highest transformation rate for the HPT-1 sample is located at 423K whereas it is located at 416K for the HPT-10 sample i.e., there is a shifting towards lower temperature. In addition, the kinetics reversion in the microstructure of the HPT-1 sample occurred at a higher rate compared with the HPT-10 one, as the maximum transformation rates of these two samples are 16×10^{-3} and 12×10^{-3} s^{-1}, respectively. This behavior is ascribed to the dissolved precipitations of smaller size, which caused them to dissolve more quickly and easily in the case of the HPT-10 sample. Additionally, for the exothermic reaction, the transformation process in the HPT-1 sample occurs at lower rate, 12×10^{-3} s^{-1} compared with that for HPT-5 (14×10^{-3} s^{-1}) and HPT-10 (18×10^{-3} s^{-1}) samples, as shown in Figure 9d-f.

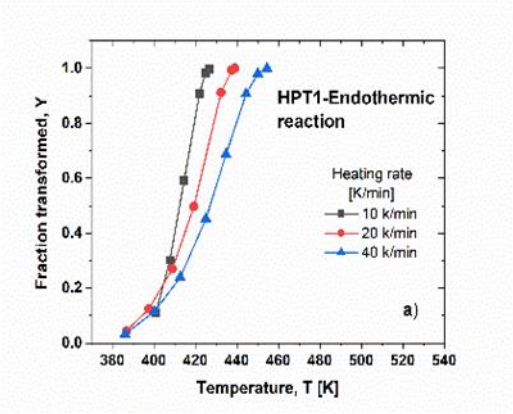

(**a**)

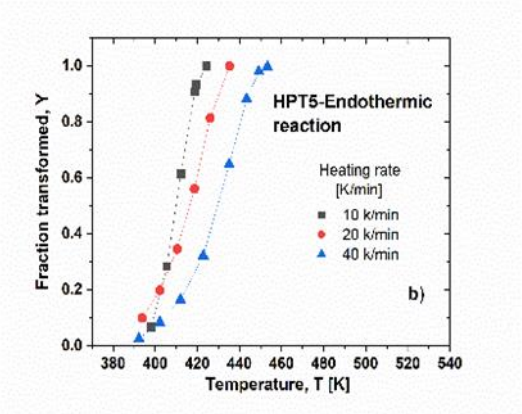

(**b**)

Preprints (www.preprints.org) | NOT PEER-REVIEWED | Posted: 29 December 2023 doi:10.20944/preprints202312.2105.v1

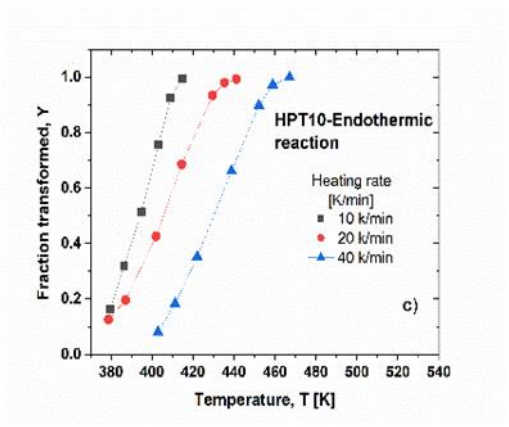

(**c**)

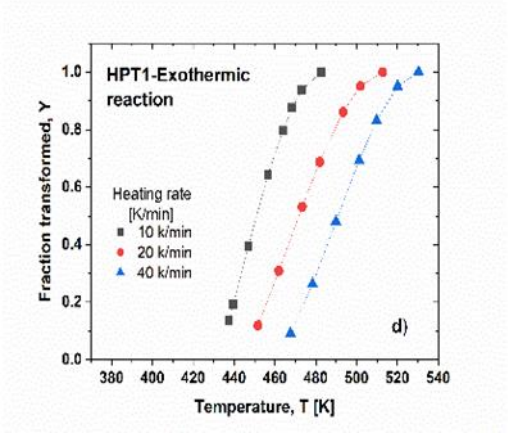

(**d**)

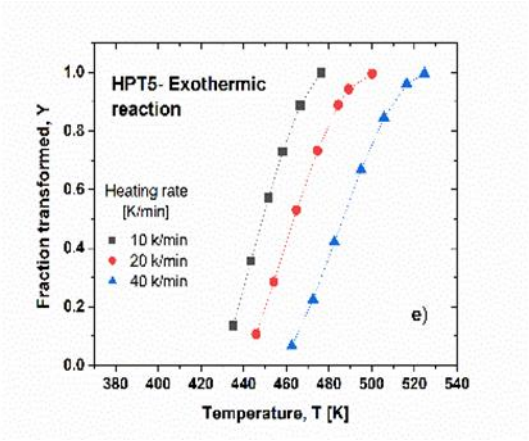

(**e**)

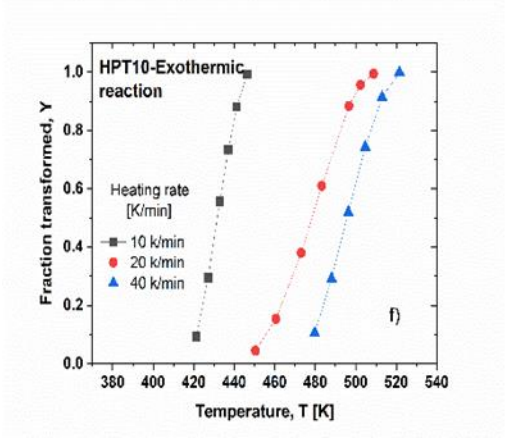

(**f**)

Figure 8. *Y-T* functions obtained at different heating rates, characterizing (**a–c**) the dissolution and (**d–f**) the precipitation reactions in HPT-1, HPT-5 and HPT-10 samples, respectively.

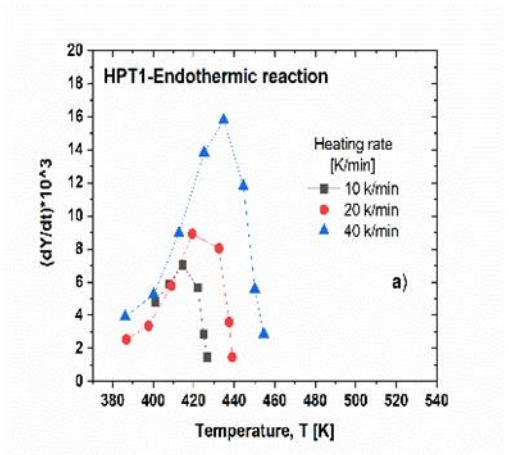

(**a**)

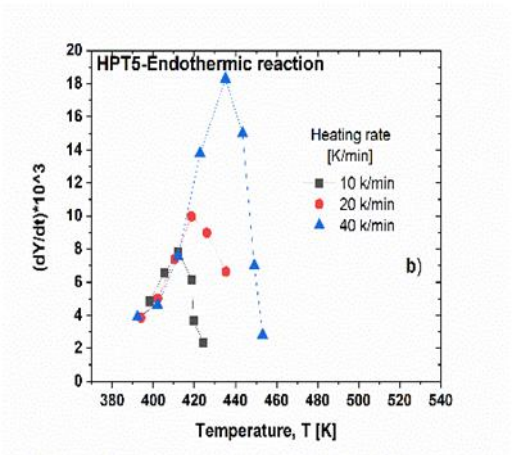

(**b**)

Preprints (www.preprints.org) | NOT PEER-REVIEWED | Posted: 29 December 2023 doi:10.20944/preprints202312.2105.v1

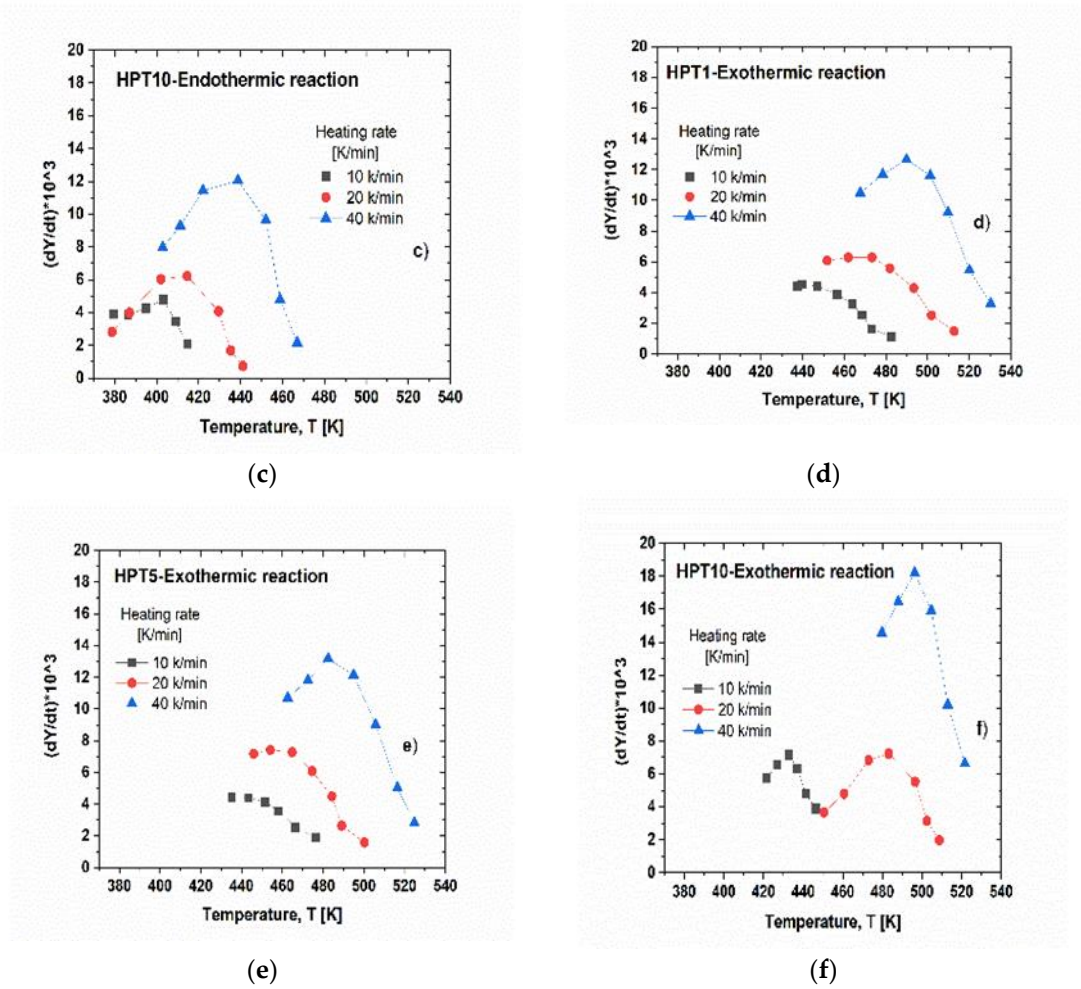

Figure 9. *dY/dt-T* plots obtained at different heating rates, describing (**a–c**) the dissolution (endothermic reaction) and (**d–f**) the precipitation (exothermic reaction) in HPT-1, HPT-5 and HPT-10 samples, respectively.

4. Discussion

Results of TEM investigations have shown that the grain-refining effect of the HPT process resulted in a stable ultrafine-grained structures having average grain size of about 200 nm in all HPT-processed samples. The strength of HPT-processed samples is primarily determined by the UFG structure, via the Hall-Petch effect [33,34], leading to almost the same hardness observed in these HPT-processed samples, as shown in Figure 1. Beside the grain-refining effect, the HPT-processing has resulted in also the decomposition of the initially supersaturated microstructure. When increasing the number of HPT revolution from 1 to 10, the decomposed microstructure has significantly changed from a structure containing only relatively large $MgZn_2$ η-phase particles to the one containing both smaller η-phase particles and high fraction of grain boundaries (GBs) segregated by solute atoms, mainly by Zn. Due to the effect of solute-segregated GBs, the creep behavior of the investigated HPT-processed samples deformed by tensile test at 170 oC strongly depends on the number of HPT revolutions. While the HPT-1 sample shows a very poor elongation lower than 50%, the HPT-10 one can be deformed superplastically with an elongation higher than 500%, under the same conditions.

Results of DSC measurements have already confirmed the significant difference between the precipitate structure formed in the HPT-10 and that in the other samples processed in smaller evolutions. The relatively high activation energy Q_d values obtained for the dissolution (endothermic) reactions in HPT-1 and HPT-2 (see Figure 7a) after low revolutions in HPT processing are related to the fragmentation of undissolved coarse η phase due to the abundance of this phase because these

Preprints (www.preprints.org) | NOT PEER-REVIEWED | Posted: 29 December 2023 doi:10.20944/preprints202312.2105.v1

samples were applied to low-strain energy. On the contrary, the relatively high, 10 evolutions lead to the dissolution of this fragmented intermetallic compounds of the η phase into the Al matrix in the HPT-10 sample, due to the high deformation energy. The low activation energy Q_d value characterizing the dissolution (endothermic) reactions in the HPT-10 sample is caused mainly by the dissolution of the low fraction of η phase which remained at grain boundaries because the dissolution of precipitates inside the grains is less pronounced [28]. Following the dissolution reaction at the first endothermic process, the formation/re-formation of precipitates is occurred as presented in the exothermic reaction peak in the DSC line profile. This process can be also characterized by decreasing activation energy (Q_p) at increasing number of HPT evolutions, as shown in Figure 7b. This is the consequence of the increasing volume fraction of GBs that facilitate the nucleation of precipitations by presenting surfaces of lower inter-phase boundary energy and of increasing dislocation density which promote the diffusion process [35-36].

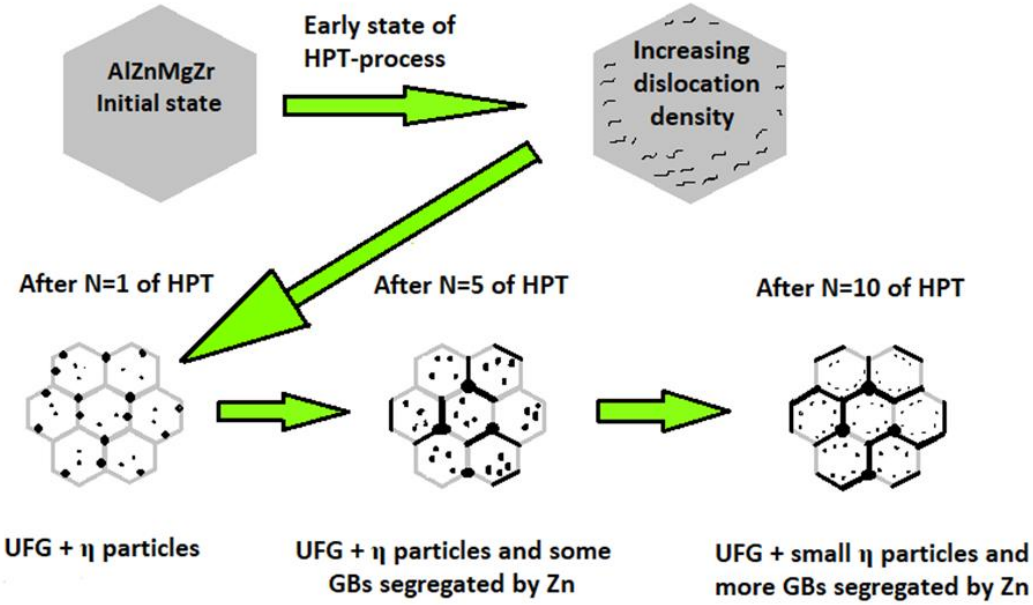

Figure 10. Schematic development of the microstructure during HPT process in 7xxx series Al-4.8Zn-1.2Mg-0.14Zr alloy.

Considering the experimental results obtained by mechanical, TEM and DSC measurements, a schematic representation on the microstructure development of the 7xxx series AlZnMg alloys during the HPT process can be suggested by main steps shown in Figure 10. It is well established that in the early stage of the HPT processing the dislocation density increases due to the intensive plastic deformation and also due to the pinning effect of the solute atoms in the initially supersaturated microstructure. The strong increase of dislocation density on the one hand, leads to the formation of an UFG structure, and on the other hand, to the decomposition of the supersaturated structure by the formation of relatively large η-phase MgZn2 particles near grain boundaries. While the UFG structure remains stable in a wide range of shear strain in HPT from one to ten evolutions, the decomposed structure is continuously changing. Due to the effect of further shear strain, the formed η-phase particles are fragmented and/or partially dissolved back into the matrix or segregated into the grain boundaries, changing significantly the creep behavior of the UFG alloy.

5. Conclusions

Microstructure and mechanical properties of an HPT-processed AlZnMgZr alloy were studied by transmission electron microscopy (TEM), differential scanning calorimetry (DSC), as well as by tensile and hardness measurements. Emphasis was placed on the effect of shear strain on the

 doi:10.20944/preprints202312.2105.v1

evolution of microstructure of the investigated alloy. The main results can be summarized as followings:

1) Severe plastic deformation exerted by HPT resulted in a stable ultrafine-grained structure having grain size of about 200 nm, increasing significantly the room temperature strength of the material.

2) Together with the formation of UFG structure, the HPT process resulted in also the decomposition of the initially supersaturated structure by the formation of η-phase MgZn2 particles near grain boundaries in the investigated AlZnMgZr alloy.

3) While the UFG structure remains stable during HPT process, the decomposed structure is continuously changing. Due to the effect of further shear strain, the formed η-phase particles are fragmented and/or partially dissolved back into the matrix or segregated into the grain boundaries. changing significantly the creep behavior of the UFG alloy.

4) The intensive segregation of solute atoms into GBs may have important role in the creep behavior of the materials, leading to its ultralow-temperature superplasticity. The obtained results pave the way for achieving advanced microstructural and mechanical properties in nanostructured metals and alloys by engineering their precipitation and segregation by means of applying different HPT revolutions.

Author Contributions: Conceptualization, A.Q.A. and N.Q.C.; methodology, A.Q.A. and N.Q.C.; validation, A.Q.A. and N.Q.C.; investigation, A.Q.A. and D.O.; writing—original draft preparation, A.Q.A. and N.Q.C.; writing—review and editing, A.Q.A., N.Q.C., E.V.B. and R.Z.V.; supervision, N.Q.C.; project administration, N.Q.C. and R.Z.V.; funding acquisition, N.Q.C. and R.Z.V.

Funding: N.Q.C. thanks the Hungarian-Russian Research program (TÉT) No. 2021-1.2.5-TÉT-IPARI-RU-2021-00001, the Hungarian Scientific Research Fund OTKA, Grant number K143216 for the research support. The work of R.Z.V. and E.V.B. was supported by the Ministry of Science and Higher Education of the Russian Federation under project No. 13.2251.21.0196 (grant agreement No. 075-15-2023-443).

Data Availability Statement: The raw and processed data required to reproduce these results are available by reasonable request.

Acknowledgments: A.Q.A. thanks the University of Kufa in Iraq for supporting and facilitating his doctoral studies at Eötvös Loránd University (ELTE). D.O. thanks the project no. C1792954 for supporting his research. Project no. C1792954 has been implemented with the support provided by the Ministry of Culture and Innovation of Hungary from the National Research, Development and Innovation Fund, financed under the KDP-2021 funding scheme.

Conflicts of Interest: The authors declare no conflict of interest.

References

1. Author 1, A.B.; Author 2, C.D. Title of the article. *Abbreviated Journal Name* **Year**, *Volume*, page range. Valiev, R.Z.; Islamgaliev, R.K.; Alexandrov, I.V. Bulk nanostructured materials from severe plastic deformation. *Prog. Mater. Sci.* **2000**, *45*, 103–189.
2. Zhilyaev, A.P.; Langdon, T.G. Using high-pressure torsion for metal processing: Fundamentals and applications. *Prog. Mater. Sci.* **2008**, *53*, 893–979.
3. Zhang, X.; Godfrey, A.; Huang, X.; Hansen, N.; Liu, Q. Microstructure and strengthening mechanisms in cold-drawn pearlitic steel wire. *Acta Mater.* **2011**, *59*, 3422–3430.
4. Kang, J.Y.; Kim, J.G.; Kim, S.K.; Chin, K.-G.; Lee, S.; Kim, H.S. Outstanding mechanical properties of high-pressure torsion processed multiscale TWIP-cored three layer steel sheet. *Scripta Mater.* **2016**, *123*, 122–125.
5. Forouzanmehr, N.; Jafarian, H.R.; Samadi-khoshkhoo, M.; Bönisch, M.; Nili-Ahmadabadi, M. Nanostructural evolution and deformation mechanisms of severely deformed pure Fe. *Met. Mater. Int.* **2021**, *27*, 1798–1807.
6. Ahmed, A.Q.; Olasz, D.; Bobruk, E.V.; Valiev, R.Z.; Chinh, N.Q. Effect of the equal channel angular pressing on the microstructure and phase composition of a 7xxx series Al-Zn-Mg-Zr alloy. *Materials* **2023**, *16(19)*, 6593.
7. Chinh, N.Q.; Murashkin, M.Y.; Bobruk, E.V.; Lábár, J.L.; Gubicza, J.; Kovács, Z.; Ahmed, A.Q.; Maier-Kiener, V.; Valiev, R.Z. Ultralow-temperature superplasticity and its novel mechanism in ultrafine-grained Al alloys. *Mater. Res. Lett.* **2021**, 9(11), 475-482.

8. Estrin, Y.; Vinogradov, A. Extreme grain refinement by severe plastic deformation: a wealth of challenging science. *Acta Mater.* **2013**, *61*, 782–817.
9. Sabirov, I.; Murashkin, M.Y.; Valiev, R.Z. Nanostructured aluminium alloys produced by severe plastic deformation: new horizons in development. *Mater. Sci. Eng. A* **2013**, *560*, 1–24.
10. Valiev, R.Z.; Estrin, Y.; Horita, Z.; Langdon, T.G.; Zehetbauer, M.J.; Zhu, Y. Producing bulk ultrafine-grained materials by severe plastic deformation: ten years later. *JOM* **2016**, *68*, 1216–1226.
11. Zhao, Y.; Zhu, Y.; Lavernia, E. J. Strategies for improving tensile ductility of bulk nanostructured materials. *Adv. Eng. Mater.* **2010,** *12(8)*, 769–778.
12. Edalati, K.; Hashiguchi, Y.; Pereira, P.H.R.; Horita, Z.; Langdon, T.G. Effect of temperature rise on microstructural evolution during high-pressure torsion. *Mater. Sci. Eng. A* **2018**, *714*, 167–171.
13. Degtyarev, M.V.; Chachchukhina, T.I.; Voronova, L.M.; Patselov, A.M.; Pilyugin, V.P. Influence of the relaxation processes on the structure formation in pure metals and alloys under high-pressure torsion. *Acta Mater.* **2007**, *55*, 6039–6050.
14. Ramalingam, V.V.; Ramasamy, P.; Kovukkal, M.D.; Myilsamy, G. Research and development in magnesium alloys for industrial and biomedical applications: a review. *Met. Mater. Int.* **2020**, *26*, 409–430.
15. Dos Santos, I.C.; Mazzer, E.M.; Figueiredo, R.B.; Langdon, T.G.; Pereira, P.H.R. Evidence for two-stage hardening in an Al-Zn-Mg-Cu alloy processed by high-pressure torsion. *J. Alloys Compd.* **2023**, *941*, 168839.
16. Khajouei-Nezhad, M.; Paydar, M.H.; Shirazi, M.M.H.; Gubiza, J. Microstructure and tensile nehavior of Al7075/Al composites consolidated from machining chips using HPT: a way of solid-state recycling. *Met. Mater. Int.* **2020**, *26*, 1881–1898.
17. Bazarnik, P.; Huang, Y.; Lewandowska, M.; Langdon, T.G. Enhanced grain refinement and microhardness by hybrid processing using hydrostatic extrusion and high-pressure torsion. *Mater. Sci. Eng. A* **2018**, *712*, 513–520.
18. Shi, S.; Zhang, Z.; Wang, X.; Zhou, G.; Xie, G.; Wang, D.; Chen, X.; Ameyama, K. Microstructure evolution and enhanced mechanical properties in SUS316LN steel processed by high pressure torsion at room temperature. *Mater. Sci. Eng. A* **2018**, *711*, 476–483.
19. Zhang, Y.; Jin, S.; Trimby, P.W.; Liao, X.; Murashkin, M.Y.; Valiev, R.Z.; Liu, J.; Cairney, J.M.; Ringer, S.P.; Sha, G. Dynamic precipitation, segregation and strengthening of an Al-Zn-Mg-Cu alloy (AA7075) processed by high-pressure torsion. *Acta Mater.* **2019**, *162*, 19–32.
20. Sha, G.; Tugcu, K.; Liao, X.Z.; Trimby, P.W.; Murashkin, M.Y.; Valiev, R.Z.; Ringer, S.P. Strength, grain refinement and solute nanostructures of an Al–Mg–Si alloy (AA6060) processed by high-pressure torsion. *Acta Mater.* **2014**, *63*, 169–179.
21. Watanabe, K.; Matsuda, K.; Ikeno, S.; Yoshida, T.; Murakami, S. TEM observation of precipitate structures in Al–Zn– Mg alloys with addition of Cu/Ag. *Metall. Mater.* **2015,** *60*, 977–979.
22. Gubicza, J.; El-Tahawy, M.; Lábár, J.L.; Bobruk, E.V.; Murashkin, M.Y.; Valiev, R.Z.; Chinh, N.Q. Evolution of microstructure and hardness during artificial aging of an ultrafine-grained Al-Zn-Mg-Zr alloy processed by high pressure torsion. *J. Mater. Sci.* **2020**, *55*, 16791–16805.
23. Pharr, G.M.; Oliver, W.C.; Brotzen, F.R. On the generality of the relationship among contact stiffness, contact area, and elastic modulus during indentation. *J. Mater. Res.* **1992,** 7, 613–617.
24. Oliver, W.C.; Pharr, G.M. An improved technique for determining hardness and elastic modulus using load and displacement sensing indentation experiments. *J. Mater. Res.* **1992,** 7, 1564–1583.
25. Chinh, N.Q.; Gubicza, J.; Langdon, T.G. Characteristics of face-centered cubic metals processed by equal-channel angular pressing. *J. Mater. Sci.* **2007**, *42*, 1594–1605.
26. Afify, N.; Gaber, A.F.; Abbady, G. Fine scale precipitates in Al-Mg-Zn alloys after various aging temperatures. *Mater. Sci. Appl.* **2011**, *2(05)*, 427.
27. Jiang, X.J.; Tafto, J.; Noble, B.; Holme, B.; Waterloo, G. Differential scanning calorimetry and electron diffraction investigation on low-temperature aging in Al-Zn-Mg alloys. *Metall. Mater. Trans. A* **2000,** *31*, 339–348.
28. Mazilkin, A.A.; Straumal, B.B.; Protasova, S.G.; Kogtenkova, O.A.; Valiev, R.Z. Structural changes in aluminum alloys upon severe plastic deformation. *Phys. Solid State* **2007**, *49*, 868–873.
29. Yannacopoulos, S.; Kasap, S.O.; Hedayat, A.; Verma, A. An experimental study of phase transformations in an Al–Zn–Mg–Zr alloy: DSC and hot microhardness measurements. *Can. Metall. Q.* **1994**, *33(1)*, 51–60.
30. Starink, M.J.; Gao, N.; Furukawa, M.; Horita, Z.; Xu, C.; Langdon, T.G. Microstructural developments in a spray-cast Al-7034 alloy processed by equal-channel angular pressing. *Rev. Adv. Mater. Sci.* **2004**, *7(1)*, 1–12.
31. Hutchinson, C.R. Modeling the kinetics of precipitation in aluminium alloys. In *Fundamentals of Aluminium Metallurgy*; Lumley, R., Ed.; Woodhead Publishing Limited: Cambridge, UK, 2011; pp. 422–467.
32. Ahmed, A.Q.; Ugi, D.; Lendvai, J.; Murashkin, M.Y.; Bobruk, E.V.; Valiev, R.Z.; Chinh, N.Q. Effect of Zn content on microstructure evolution in Al–Zn alloys processed by high-pressure torsion. *J. Mater. Res.* **2023**, *38(14)*, 3602–3612.
33. Hall, E.O. Variation of hardness of metals with grain size. *Nature* **1954**, *173*, 948–949.
34. Petch, N.J. The cleavage strength of polycrystals. *J. Iron Steel Inst.* **1953**, *174*, 25–28.

35. Miesenberger, B.; Kozeschnik, E.; Milkereit, B.; Warczok, P.; Povoden-Karadeniz, E. Computational analysis of heterogeneous nucleation and precipitation in AA6005 Al-alloy during continuous cooling DSC experiments. *Materialia* **2022**, *25*, 101538.
36. Zhao, Y.H.; Liao, X.Z.; Cheng, S.; Ma, E.; Zhu, Y.T. Simultaneously increasing the ductility and strength of nanostructured alloys. *Adv. Mater.* **2006**, *18(17)*, 2280–2283.